DOI: https://doi.org/10.68732/b70332a0ba714a9a

ISBN: 978-9989-2053-7-8

Deterministic DFN Modelling and Analysis of Large Caverns at 1000 m Depth

A. Rahnama & D. Saiang
Luleå University of Technology, Mining and Rock engineering, Luleå, Sweden
ali.rahnama@ltu.se
0009-0005-3285-4806

Abstract

Underground excavations are commonly classified into normal, wide, very-wide, and super-wide span categories. Very-wide and super-wide excavations include hydropower machine halls, large mining chambers, underground research laboratories, and specialized underground storage facilities. As span increases, the mechanical response of the surrounding rock mass may depart from conventional tunnel-scale behaviour, with greater sensitivity to stress redistribution, discontinuity-controlled deformation, block formation, and localized yielding. This paper investigates the stability response of the proposed ESSnuSB Far Detector cavern system, consisting of large dome-shaped caverns with a diameter of about 78 m, located at approximately 1000 m depth in hard rock. A three-dimensional continuum-based finite-element model was developed, and a deterministic joint network was introduced to examine the influence of joint spacing, persistence, and orientation. The response was evaluated using displacement, yielded-zone development, stress redistribution, and relative joint shear displacement. The results show that finite discontinuities can modify both the magnitude and spatial distribution of the cavern response compared with the equivalent continuum reference model. Spacing and persistence produced a non-monotonic response controlled by fracture intensity, finite joint size, joint continuity, and three-dimensional rock-bridge interaction, while joint orientation showed a more systematic influence on displacement and joint shear displacement. The findings indicate that deterministic joint-network modelling provides useful insight into large cavern stability where joint geometry, excavation-boundary interaction, and stress redistribution interact.

Keywords

Large span excavation, Discrete fracture network, Continuum modelling, Deep underground opening.

1 Introduction

Large-span underground excavations are used in hydropower, underground storage, research, transport, and public facilities, where the required functional volume becomes a primary design constraint (Lindblom et al. 2018). Their stability is controlled by in-situ and induced stresses, excavation geometry, rock strength, and rock mass structure. In deep jointed rock masses, stress redistribution and discontinuity-controlled mechanisms may promote localized yielding, sliding, wedge release, and block rotation (Diederichs 2007; Goodman and Shi 1985).

Hoek and Brown (1980) and Brady and Brown (2004) classify excavations into normal, wide, very-wide, and super-wide span categories, with super-wide spans generally exceeding 30 m. For very large caverns, rock mass classification and equivalent-continuum approaches remain useful for preliminary assessment, but they describe discontinuities mainly through averaged parameters rather than location-specific geometry (Barton et al. 1974). This limitation becomes important where joint spacing, persistence, orientation, and finite joint size are comparable to the excavation scale. Deterministic joint-network modelling can retain these geometric attributes and evaluate their influence on displacement, yielded-zone development, stress redistribution, and relative joint shear displacement (Wei et al. 2022).

This paper investigates the proposed ESSnuSB Far Detector cavern, consisting of two large dome-shaped caverns at about 1000 m depth in hard rock (Rahnama et al. 2025). A three-dimensional continuum-based finite-element model with a deterministic joint network is used to evaluate the influence of joint spacing, persistence, and orientation on the cavern response.

2 Case description and input parameters

The proposed ESSnuSB Far Detector cavern system consists of two large dome-shaped caverns, each about 78 m in diameter and 100 m high, located at an approximate depth of 1000 m (Rahnama et al. 2025). As shown in Fig. 1, this combination of span, height, and depth places the caverns near the upper range of current large-span underground excavation experience. The caverns are planned close to an active mine, where existing underground access and infrastructure provide the practical setting for the conceptual study. Previous work indicated that a stand-off distance of about 250 m is needed to place the caverns outside the main area of mine influence (Saiang 2019).

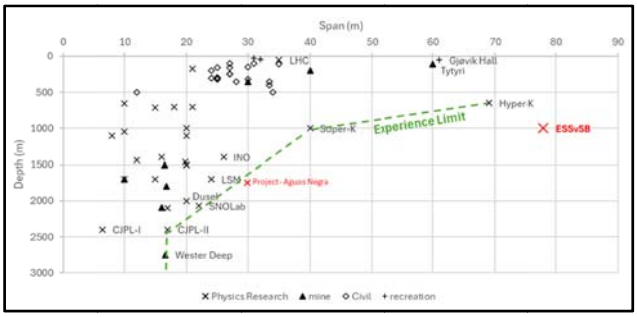


Fig. 1 The experience of large underground Structures (Montano Atencio 2024; Rahnama et al. 2025).

Rock mass input parameters were adopted from the site model used by Rahnama et al. (2025). The model includes the limestone/marble footwall, copper ore, and quartz-feldspar leptite hanging-wall units, with the proposed caverns located mainly within the limestone/marble unit. The reported GSI range for the limestone/marble is 60–65, and the corresponding rock mass strength and deformation parameters are summarized in Table 1.

Table 1. Rock Mass Properties (Daffern et al. 2017; Rahnama et al., 2025).

Rock Type	Strength	mi	σ_c (MPa)	GSI	c (MPa)	φ (°)	σ_{tm} (MPa)
Limestone/marble (Cu footwall)	Typical	12	100	65	5.9	38.4	0.6
Copper Ore	Typical	20	165	60	7.3	45.5	0.4
Quartz-feldspar leptite (Cu hanging wall)	Typical	25	300	75	13.3	55.7	1.8

mi = Hoek–Brown intact rock parameter; σ_c = uniaxial compressive strength of intact rock; GSI = Geological Strength Index; c and φ = Mohr–Coulomb rock mass cohesion and friction angle; σ_{tm} = uniaxial tensile strength of the rock mass.

The in-situ stress field was represented using two available site interpretations: overcoring and hydraulic fracturing. Both indicate a high-stress environment, with σ_H oriented approximately north–south, σ_h approximately east–west, and σv following the overburden direction. The corresponding stress-depth relations are summarized in Table 2.

Table 2. Stress depth relation (Saiang 2019).

Method	Major horizontal stress, σH	Minor horizontal stress, σh	Vertical stress, σv
Overcoring	σ_H = 0.068z, N–S	σh = 0.047z, E–W	σv = 0.028z
Hydraulic fracturing	σH = 2.8 + 0.04z, N–S	σh = 2.2 + 0.024z, E–W	σv = 0.027z

3 Numerical Modelling

At the planned cavern depth, the hydraulic-fracturing interpretation gives a maximum stress of about 40–45 MPa, whereas the overcoring interpretation gives about 65–72 MPa (Saiang 2019). The hydraulic-fracturing stress state was therefore adopted as the reference condition for the conceptual model, as it provides a more regionally representative estimate of the in-situ stress field than overcoring.

3.1 Baseline Numerical Model

To improve computational efficiency, a symmetry-based single-cavern model was adopted for the deterministic joint-network analyses. Previous two-cavern modelling showed limited stress interaction between the caverns and confirmed that the selected cavern location remained outside the main mining-disturbed zone (Rahnama et al. 2025). One representative cavern was therefore modelled with a symmetry boundary, where displacement normal to the symmetry plane was restrained and tangential displacement was allowed. Before introducing the joint-network cases, the half model was checked against the complete 3D model and showed close agreement in principal stress distribution, cavern-induced displacement, stress redistribution, and yielded-zone pattern. The modelling sequence, including the original cavern setting, symmetry cut, and deterministic joint-network schematic, is shown in Fig. 2.

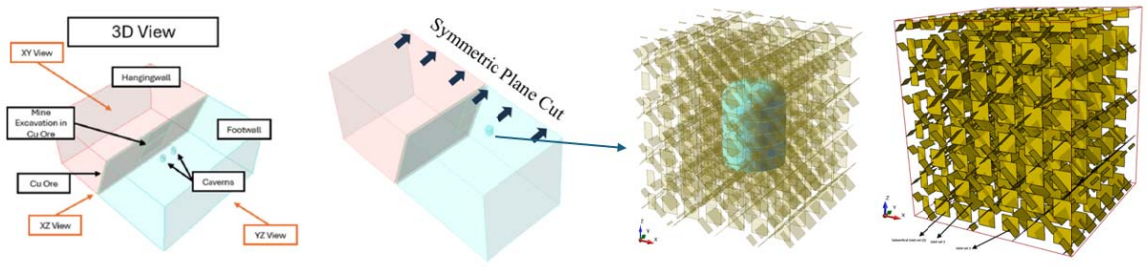


Fig 2. The original and the half symmetric model adoption (Rahnama et al. 2025) and Schematic of introduce Joint sets.

3.2 Deterministic joint-network setup and sensitivity cases

A conceptual deterministic joint network was introduced to represent finite discontinuities around the cavern. The network is not intended as a calibrated reconstruction of the site fracture system, but as a controlled three-set configuration for isolating the effects of joint spacing, persistence, and orientation. The adopted network consists of two conjugate joint sets and one vertical cross-joint set, following the common DFN description of fracture systems in terms of orientation, size, intensity, and spatial distribution (Dershowitz and Herda 1992; Lei et al. 2017).

All discontinuities were modelled as finite 20 m × 20 m quadrilateral joints within a 60 m buffer around the cavern. The selected joint size is approximately one quarter of the 78 m cavern span and is used as a scale-consistent conceptual value, not as a measured fracture length. The 60 m buffer corresponds to about three times the joint length and is consistent with the representative-volume concept proposed by Oda (1988). Because site-specific persistence data were unavailable, persistence was treated as a sensitivity parameter. A baseline value of P = 0.50 was used to represent an intermediate non-persistent joint system where both finite joint patches and rock bridges remain mechanically relevant (Shang et al. 2018; Cao et al. 2022).

Because direct shear tests, JRC/JCS measurements, and joint wall strength data were unavailable, the joints were treated as open frictional discontinuities using a perfectly plastic Mohr–Coulomb law:

$$\tau_{max} = c_j + \sigma_n \tan \varphi_j$$

where τ_{max} is the available shear resistance, c_j is joint cohesion, σ_n is the normal stress acting on the joint plane, and φ_j is the joint friction angle.

The adopted joint parameters were zero cohesion, zero tensile strength, φ_j = 28°, zero dilation, and residual values equal to peak values. This simplified joint law is appropriate for a comparative sensitivity study where joint geometry is the main variable and detailed joint surface data are unavailable (Cundall et al. 2008; Barton and Choubey 1977).

The deterministic joint-network analyses were designed as a comparative sensitivity study. The rock mass properties, in-situ stress field, cavern geometry, joint size, and joint mechanical parameters were kept constant, while joint spacing, persistence, and orientation were varied separately. The response was evaluated using maximum displacement, yielded-zone extent, yielded-zone pattern, stress redistribution, and relative joint shear displacement. The joint-network assumptions and sensitivity cases are summarized in Table 3.

Table 3. Deterministic joint-network assumptions and sensitivity cases.

Parameter	Adopted value(s) / levels	Interpretation / fixed inputs
Joint set orientations	J1: 45°/90°; J2: 45°/270°; J3: 90°/0°	Two conjugate sets and one vertical cross-joint set
Joint geometry and buffer	20 m × 20 m quadrilateral joints; 60 m buffer	Finite joints in RS3; joint length ≈ 0.25 of cavern span
Joint properties and baseline	$c_j = 0$; $\varphi_j = 28°$; dilation = 0°; tensile strength = 0; P = 0.50	Open frictional joints; residual = peak; intermediate baseline persistence
Spacing sensitivity series	40 m, 30 m, 15 m, 10 m	P = 0.50; reference orientation; fixed joint size and mechanics
Persistence sensitivity series	0.25, 0.50, 0.75	Spacing = 15 m; reference orientation; fixed joint size and mechanics
Orientation sensitivity series	0°, 45°, 90° plan rotation	Spacing = 15 m; P = 0.50; fixed joint size and mechanics

4 Results

4.1 Model verification

The numerical model was first checked against the available in-situ stress interpretations at the planned cavern depth. The modelled major and minor principal stresses showed close agreement with the hydraulic-fracturing interpretation adopted as the reference stress condition (Fig. 3). Because the caverns have not yet been constructed, no monitoring data were available for further calibration; therefore, verification was limited to the initial stress field and the reference continuum response.

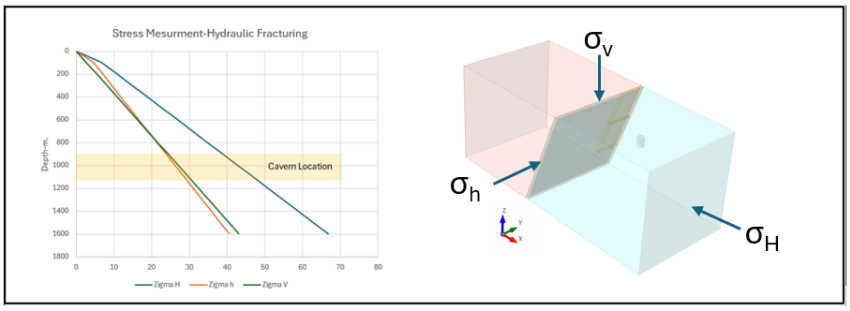


Fig. 3Principal Major (Zh) and Minor stress (Zh) Plot versus dept and schematic orientation in Numerical Model.

4.2 Effect of joint spacing

The first sensitivity series examined the influence of joint spacing on cavern response. Four spacing intervals were compared: 40 m, 30 m, 15 m, and 10 m. These intervals were interpreted relative to the cavern span using R = Js/S, where Js is the joint spacing and S = 78 m is the cavern span. Joint size, persistence, orientation, and mechanical properties were kept constant, so spacing was the only variable.

The principal stress redistribution was also checked, but no major change in the larger-scale stress pattern was observed. The influence of spacing was therefore more clearly expressed through displacement localization and yielded-zone development. The displacement contours show broadly similar deformation patterns, but different displacement magnitudes and local concentrations near the cavern boundary (Fig. 4). Yielding remains concentrated around the crown, sidewalls, and cavern base in all cases, although its extent and continuity vary with spacing (Fig. 5). As summarized in Table 4, the 15 m spacing case produced the largest maximum displacement and crown yielded-zone extent, whereas the 10 m spacing case produced the largest yielded-zone extent at the cavern base. This indicates a non-monotonic spacing response controlled by the interaction between finite joints, excavation-boundary intersection, and local stress redistribution. Table 4 summarizes the results of the joint spacing cases in terms of the spacing ratio (R), maximum displacement, and yielded zone extent at the crown and bottom of the cavern.

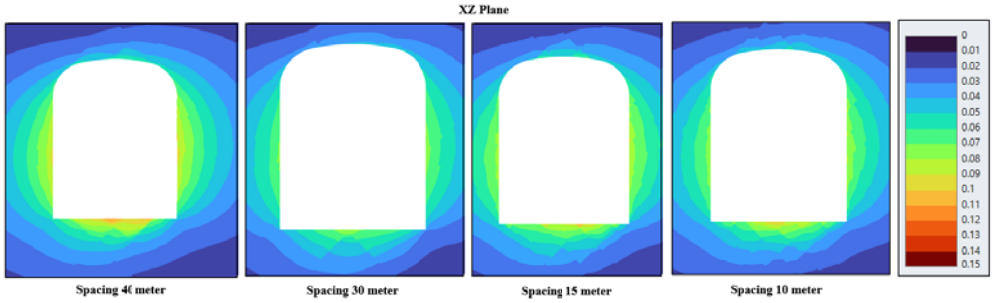


Fig. 4 Total displacement contours for the joint spacing cases for XZ.

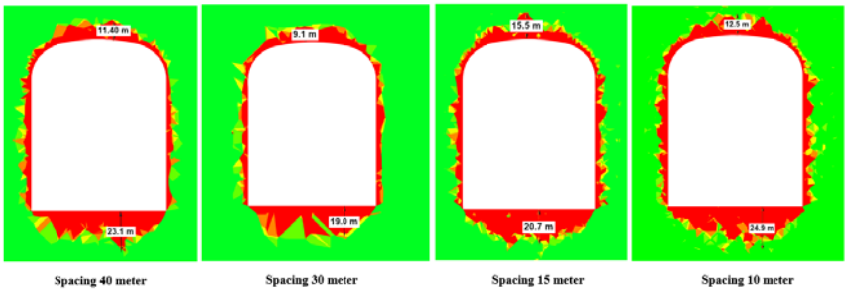


Fig. 5 Yielded zones comparison in the XZ section for the joint spacing cases in meter.

Table 4. Summary of maximum displacement and yielded zone extent for the joint spacing cases.

Case	Joint spacing, J_s	R = J_s/S	Max. Disp. (m)	Crown yield zone extent. (m)	Base yield zone extent. (m)
S40	40 m	0.51	0.10	11.40	23.07
S30	30 m	0.38	0.09	9.07	19.04
S15	15 m	0.19	0.14	15.52	20.74
S10	10 m	0.13	0.13	12.52	24.88

4.3 Joint persistence analysis

The persistence sensitivity analysis examined the influence of joint continuity on cavern response. Joint spacing was kept constant at 15 m, based on the critical spacing case identified in the previous series, while persistence was varied as P = 0.25, 0.50, and 0.75. The evaluation focused on total displacement and yielded-zone extent, with the main quantitative results summarized in Table 5.

The displacement contours show that the three persistence cases retain a similar overall deformation pattern, but the displacement magnitude and localization vary with joint continuity (Fig. 6). The yielded-zone results also show a non-monotonic response (Fig.7). The P = 0.50 case gives the largest maximum displacement and crown yielded-zone extent, whereas the P = 0.75 case gives the largest yielded-zone extent at the cavern base. The XY views were also checked and showed a broadly circumferential yielded band around the cavern boundary in all cases. This indicates that persistence mainly changes the local thickness and irregularity of the yielded zone, rather than producing a fundamentally different plan-view failure pattern.

Table 5. Summary of maximum displacement and yielded zone extent for the joint persistence cases.

Case	Persistence, P	Max. displacement (m)	Crown yield. extent (m)	Floor yield. extent (m)
P025	0.25	0.10	11.086	22.547
P050	0.50	0.14	15.518	20.741
P075	0.75	0.12	14.322	22.992

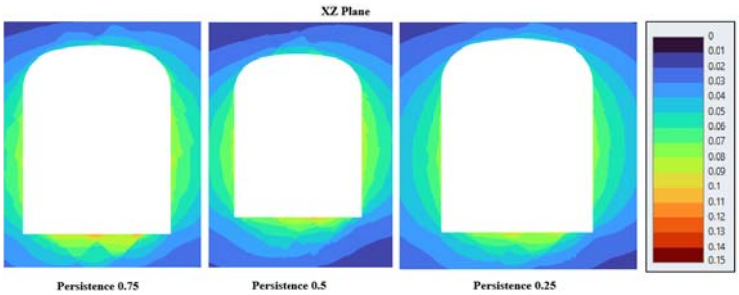


Fig. 6 Total displacement contours for the joint persistence cases at the XY and XZ planes.

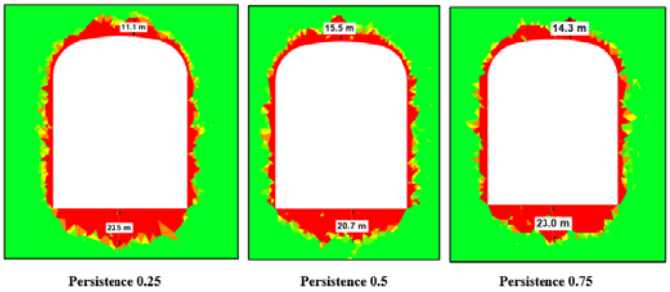


Fig. 7 Yielded zone comparison in the XZ section for the joint persistence cases.

4.4 Effect of joint orientation

The orientation sensitivity analysis examined the effect of rotating the complete three-set joint network relative to the principal horizontal stress field. Joint spacing was kept constant at 15 m and persistence at P = 0.50, while joint size, mechanical properties, cavern geometry, and in-situ stress magnitudes were unchanged. The three cases represent σ_1-parallel, 45° intermediate, and σ_2-parallel joint orientations.

The results show a systematic reduction in both maximum displacement and relative joint shear displacement as the joint setting is rotated away from the σ_1-parallel reference condition (Table 6). The displacement contours confirm this trend for the rotated cases (Fig. 8). Yielding remains generally circumferential around the cavern boundary, although the local yielded-zone distribution changes with orientation (Fig. 9). Relative joint shear displacement follows the same pattern, with the highest mobilization in the σ_1-parallel case, an intermediate response in the 45° case, and the lowest mobilization in the σ_2-parallel case (Fig. 10).

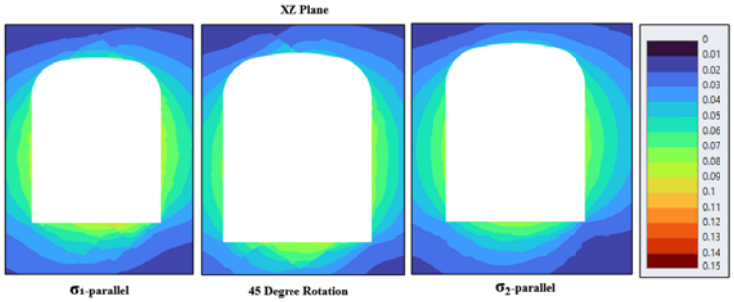


Fig. 8 Total displacement contours for the joint setting orientation.

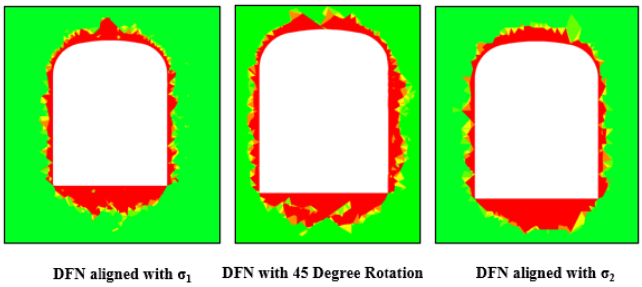


Fig. 9 XZ yielded zone pattern for the σ_2-aligned and 45 degree rotation joint orientation.

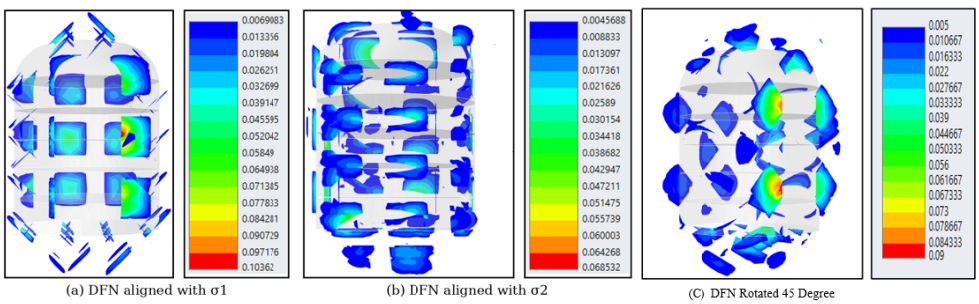


Fig. 10 Relative shear displacement along joints for the three joint orientations (m.).

Table 6. Effect of joint orientation on displacement and joint shear displacement.

Case	Joint orientation	Rotation	Max. disp. (m)	Max. joint shear (m)	Observation
R0	Parallel to σ_1	0°	0.14	0.10	Reference case
R45	Intermediate	45°	0.11	0.09	Reduced displacement and joint shear
R90	Parallel to σ_2	90°	0.10	0.06	Lowest displacement and joint shear

5 Discussion

Figure 1 shows the exceptional scale of the proposed ESSnuSB far detector caverns relative to existing large underground openings experience. With a span of 78 m and a depth of about 1000 m, the case lies near the upper range of current large-cavern experience. This scale makes the location-specific geometry of finite discontinuities important, because joint spacing, persistence, and orientation may interact directly with the excavation boundary and induced stress field. The deterministic joint-network analyses were therefore used as a controlled sensitivity framework to evaluate how discontinuity geometry modifies displacement localization, yielded-zone development, and joint-controlled movement around the cavern.

5.1 Joint Spacing & Persistence

The spacing and persistence results show that the cavern response is not governed by a simple monotonic trend. In the spacing series, the 15 m case produced the largest maximum displacement and crown yielded extent, whereas the 10 m case produced the largest yielded extent at the cavern base. In the persistence series, P = 0.50 produced the largest maximum displacement and crown yielded extent, while the more continuous P = 0.75 case did not produce the maximum displacement. These results indicate that the critical response is controlled not only by fracture intensity or persistence alone, but by the combined effect of finite joint size, boundary intersection, joint continuity, and remaining rock bridges. In a three-dimensional finite-joint model, persistence therefore does not act only as a two-dimensional continuity ratio; rock bridges and the spatial arrangement of joint patches can still maintain load transfer and delay the formation of fully connected failure paths.

5.2 Joint Orientation

The joint orientation results show a more consistent trend than the spacing and persistence cases. Rotating the joint set away from the σ_1-parallel reference condition reduced both maximum displacement and maximum relative joint shear displacement. This indicates that joint orientation relative to the principal stress field directly influences deformation and shear mobilization along the joints. However, yielding remained generally circumferential around the cavern boundary in all orientation cases. The main orientation effect is therefore interpreted as a redistribution of local yielding and a reduction in joint-controlled movement, rather than a complete change in the yielded-zone mechanism.

5.3 Comparison with the continuum reference model

Comparison with the continuum plastic reference model further shows the influence of the deterministic joint network. In the reference model, the maximum displacement was about 0.072 m and the yielded zone was comparatively regular, with yielded depths generally between about 7 m and 15 m (Montano Atencio 2024). In the deterministic joint-network cases, the maximum displacement increased to 0.14 m, and the yielded zone became more irregular and locally deeper, with crown and base extents reaching about 15.5 m and 24.9 m, respectively. This comparison indicates that finite joint geometry affects not only the magnitude of the response, but also the spatial distribution of deformation and yielding around the excavation.

6 Conclusion

This study examined how deterministic joint spacing, persistence, and orientation influence the stability response of the proposed ESSnuSB Far Detector cavern, a 78 m diameter cavern located at about 1000 m depth in hard rock. Compared with the equivalent continuum plastic reference model, the deterministic joint-network cases produced higher displacement and more irregular yielded-zone development. The maximum displacement increased from about 0.072 m in the reference model to 0.14 m in the critical joint case, indicating that averaged continuum parameters may underrepresent local structural effects at this cavern scale.

The spacing and persistence analyses showed a non-monotonic response controlled by fracture intensity, finite joint size, joint continuity, boundary intersection, and three-dimensional rock-bridge interaction. In contrast, the orientation analysis showed a more systematic trend, where rotating the joint set away from the σ_1-parallel reference condition reduced both maximum displacement and relative joint shear displacement, while yielding remained generally circumferential around the cavern boundary.

The model should be interpreted as a continuum-based deterministic joint-parameter sensitivity analysis, not as a full discrete-element simulation of block movement or post-failure separation. Within this limitation, the results show that deterministic joint-network modelling can provide useful additional insight into large-span cavern stability where joint geometry, excavation-boundary interaction, and stress redistribution are important.

References

Barton N, Choubey V (1977) The shear strength of rock joints in theory and practice. Rock Mechanics 10:1–54.

Barton N, Lien R, Lunde J (1974) Engineering classification of rock masses for the design of tunnel support. Rock Mechanics 6:189–236.

Brady BHG, Brown ET (2004) Rock mechanics for underground mining. 3rd edn. Springer, Dordrecht.

Cao R, Dai H, Yao R, Lin H, Li K (2022) Failure behaviour of jointed rock masses with 3D nonpenetrating joints under uniaxial compression: Insights from discrete element method modelling. Applied Sciences 12:11027.

Cundall PA, Pierce ME, Mas Ivars D (2008) Quantifying the size effect of rock mass strength. First Southern Hemisphere International Rock Mechanics Symposium (SHIRMS 2008), Perth, Australia.

Daffern T, Ellis R, King P, Richardson S, Glücksman E, Beveridge A (2017) NI 43-101 technical report for the Zinkgruvan Mine, Sweden. Lundin Mining Corporation.

Dershowitz WS, Herda HH (1992) Interpretation of fracture spacing and intensity. 33rd U.S. Symposium on Rock Mechanics, Santa Fe, New Mexico.

Diederichs MS (2007) The 2003 Canadian Geotechnical Colloquium: Mechanistic interpretation and practical application of damage and spalling prediction criteria for deep tunnelling. Canadian Geotechnical Journal 44(9):1082–1116.

Goodman RE, Shi GH (1985) Block theory and its application to rock engineering. Prentice-Hall, Englewood Cliffs.

Hoek E, Brown ET (1980) Underground excavations in rock. Institution of Mining and Metallurgy, London.

Lei Q, Latham JP, Tsang CF (2017) The use of discrete fracture networks for modelling coupled geomechanical and hydrological behaviour of fractured rocks. Computers and Geotechnics 85:151–176.

Lindblom U, Ericsson LO, Winqvist T, Tengborg P, Håkansson U (eds) (2018) Sweden underground: Rock engineering and how it benefits society. BeFo Rock Engineering Research Foundation and Swedish Rock Engineering Association, Stockholm.

Montano Atencio JA (2024) Stability analysis on the proposed excavation ESSvSB caverns. Master's thesis, New Mexico Institute of Mining and Technology.

Oda M (1988) A method for evaluating the representative elementary volume based on joint survey of rock masses. Canadian Geotechnical Journal 25(3):440–447.

Rahnama A, Saiang D, Montano Atencio JA (2025) Stability analysis of large underground caverns of unprecedented dimensions at depth. 59th U.S. Rock Mechanics/Geomechanics Symposium, Santa Fe, New Mexico, USA.

Saiang D (2019) Pre-study of candidate site for underground infrastructure for neutrino research. UNRI project report. Luleå University of Technology, Luleå.

Shang J, West LJ, Hencher SR, Zhao Z (2018) Geological discontinuity persistence: Implications and quantification. Engineering Geology 241:41–54.

Wei S, Li Y, Shang Y, Sun Y, Li K (2022) Stability analysis of fractured rock mass around underground excavations based on a three-dimensional discrete fracture network. Environmental Earth Sciences 81:65.